Electronic Supplementary Material (ESI) for Journal of Materials Chemistry A.

Supporting Information

Thermally-Assisted Photocatalytic Conversion of CO_2-H_2O to Ethylene over Carbon Doped In_2S_3 Nanosheets

Lei Wang,‡[a] Bohang Zhao,‡[a] Changhong Wang,[a] Mengyao Sun,[a] Yifu Yu[a] and Bin Zhang*[ab]

[a]Department of Chemistry, School of Science, Institute of Molecular Plus, Tianjin University, Tianjin 300072, China

[b]Tianjin Key Laboratory of Molecular Optoelectronic Sciences, Tianjin University, Tianjin 300072, China

‡These authors contributed equally.

*E-mail: bzhang@tju.edu.cn

1. Experimental section.

1.1 Chemicals. Indium chloride ($InCl_3 \cdot 4H_2O$), L-cysteine, triethylenetetramine (TETA) and thiourea were purchased from Aladdin Ltd. The carbon dioxide (CO_2) gas was bought from Air Liquide (Tianjin) Co. Ltd. Deionized water (DIW) was used in all the experimental processes. All chemicals were of analytical grade and used without further purification.

1.2 Synthesis of carbon doping In_2S_3 (C-In_2S_3). The organic-inorganic hybrid precursor InS-TETA was synthesized by our previous method.[1] 0.2212 g $InCl_3 \cdot 4H_2O$ and 0.7269 g L-cysteine were dissolved in 12 mL H_2O and 6 mL TETA (triethylenetetramine) in an aqueous solution, stirred vigorously for 30 minutes, and then transferred to a 25 mL Teflon-lined stainless steel autoclave. The mixture was heated to 160 °C for 24 hours, then naturally cooled to room temperature. At the end of the reaction, the white product formed was washed three times with deionized water and absolute ethanol and placed in a vacuum drying oven for drying. The obtained organic-inorganic hybrid is called InS-TETA. 10 mg as-prepared hybrid InS-TETA was put into a solvent of 12 mL DIW in a 20 mL Teflon-lined stainless-steel autoclave under vigorous stirring for 30 minutes to form a homogeneous solution. The autoclave was sealed and kept at 180 °C for 10 h. The yellow precipitate was washed by DIW and absolute ethanol, respectively, and dried in a vacuum oven to obtain C-In_2S_3.

1.3. Synthesis of In_2S_3. As reported in the literature,[2] 0.5863 g $InCl_3 \cdot 4H_2O$ and 0.6089 g thiourea were put in an agate and mixed uniformly. Then the mixture was placed in a 6 mm diameter quartz tube and put into a tube furnace. Then the temperature was raised to 220 °C at a heating rate of 10 °C/min under the air atmosphere for 5 minutes. Finally, it was cooled down naturally to room temperature. The as-obtained powder was washed three times with hot DIW and ethanol to remove impurities and dried in a vacuum oven to obtain an orangered solid called In_2S_3.

2. Materials Characterizations.

Powder X-ray diffraction (XRD) was performed on a Bruker D8 Focus Diffraction System using a Cu Kα source (λ=0.154178 nm). SEM was conducted with a Hitachi S-4800 scanning electron microscope equipped with the Thermo Scientific energy-dispersion X-ray fluorescence analyzer. TEM, HRTEM were obtained with a JEOL-2100F system equipped with an EDAX Genesis XM2. XPS measurements were conducted with a PHI-1600 X-ray photoelectron spectrometer equipped with Al Ka radiation. X-ray photoelectron spectroscopy (XPS) measurements were performed on a photoelectron spectrometer using Al Kα radiation as the excitation source (PHI 5000 VersaProbe) with or without illumination. All the peaks were calibrated with the C 1s spectrum at a binding energy of 284.8 eV. UV-Vis diffuse reflectance spectra (UV-Vis DRS) were recorded on a Lambda 750 UV-Vis spectrometer (PerkinElmer) equipped with an integrating sphere. The UV-Vis DRS spectra of solid samples were collected in 200-800 nm against $BaSO_4$ reflectance standard. Raman spectroscopy was recorded on Renishaw inVia reflex Raman microscope under an excitation of 532 nm laser light with a power of 20 mW. Ultraviolet photoemission spectroscopy (UPS) measurements were performed with an unfiltered He I (21.22 eV) gas discharge lamp and a total instrumental energy resolution of 100 meV. Spectroscopy Photoluminescence (PL) was carried out on a Supermini 200 with a 50 kV X-ray tube. *In situ* diffuse reflectance infrared Fourier transform spectroscopy (DRIFTS) analysis is carried out in a continuous-flow mode under Visible light irradiated and dark conditions, respectively, with external heating of 150 °C. And the results were calculated by the Kubelka-Munk function. The gas-phase product was measured on Agilent 7890A with thermal conductivity detector (TCD) and Shimadzu GC-2010 Plus with Barrier Discharge Ionization Detector (BID). Helium (He) was used as a carrier gas. The C_2H_4 generated by $^{13}CO_2$ and D_2O isotope experiments were analyzed by the QP2010Ultra gas chromatography-mass spectrometer.

3. Thermal assisted Photocatalytic CO_2 Conversion.

The thermal assisted photocatalytic conversion of CO_2 and H_2O was carried out in a stainless steel reaction chamber equipped with a quartz window at a chamber volume of 75 mL. Before the photoreaction, the sample (30 mg) was well dispersed in the reaction chamber, and the gas in the chamber was discharged by a mechanical pump. CO_2 was bubbled into the chamber with 0.1 mL water and reached atmospheric pressure. The products formed in the irradiated chamber were measured at regular intervals under the 300 W xenon lamp (Beijing Perfect light PLS-SXE-300UV) with the light intensity of 1 W/cm^2 and external heating at 150 °C.

When the products were subjected to barrier discharge ionization detection for gas chromatography analysis, the GC-2010 gas chromatograph equipped with an activated carbon packed column (carrier gas He) was used. The overall formula during the photocatalytic conversion of CO_2-H_2O to C_2H_4 over C-In_2S_3 is supposed to be

$$CO_2 + H_2O \longrightarrow \begin{cases} CO \\ CH_4 \\ C_2H_6 \\ C_2H_4 \\ O_2 \end{cases}.$$

The evolution rate of different products was calculated using equations (1). The selectivity of C_2H_4 among all products and hydrocarbons were calculated using equation (2) and (3).

$$\text{Evolution Rate } (\mu\text{mol}/g/h) = \frac{\text{peak area of X } \times C}{\text{peak area of standard gas} \times t \times m} \times V \qquad (1)$$

$$\text{Selectivity}(C_2H_4) = \frac{\text{Evolution Rate of } C_2H_4}{\text{Evolution Rate of all products}} \qquad (2)$$

$$\text{Selectivity}(C_2H_4) = \frac{\text{Evolution Rate of } C_2H_4}{\text{Evolution Rate of hydrocarbons}} \tag{3}$$

X : The different products including H_2, CO, CH_4, C_2H_4 and C_2H_6.

C : The concentration of X in standard gas.

t : The illumination time.

m : The mass of used catalyst.

V : The volume of used reactor.

4 The measurement of Quantum Efficiency. The Quantum Efficiency (QE) of our system is measured under external heating at 150 °C. In a typical procedure of the measurement of QE, 100 mg photocatalyst was well-dispersed in a stainless steel reaction chamber equipped with a quartz window at a chamber volume of 75 mL. CO_2 was bubbled into the chamber with 0.1 mL water and reached atmospheric pressure. 180 W Light Emitting Diode (LED) Electro Luminescent (EL) with the light intensity of 10 $mW \cdot cm^{-2}$ in the wavelength of 420 nm was used as the light source and the irradiation area was fixed to 1.0 cm^{-2} under external heating at 150 °C. The details of QE calculation were blown.

(1) The number of absorbed photons ($N_{absorbed}$):

$$N_{absorbed} = \frac{t\,(s) \times P\,(W \cdot cm^{-2}) \times \lambda\,(m)}{h\,(J \cdot s) \times c\,(m \cdot s^{-1})}$$

$$N_{absorbed} = \frac{1(s) \times 0.01(W \cdot cm^{-2}) \times 1(cm^{2}) \times 420 \times 10^{-9}(m)}{6.626 \times 10^{-34}(J \cdot s) \times 3 \times 10^{8}(m \cdot s^{-1})} = 2.1 \times 10^{16}$$

(2) The QE of CO_2 reduction was obtained by:

$$QE = \frac{(2n_{CO} + 8n_{CH_4} + 12n_{C_2H_4} + 14n_{C_2H_6})(mol) \times N_A\,(mol^{-1})}{N_{absorbed}} \times 100\,\%$$

$$QE = \frac{(2 \times 10.04 \times 10^{-11} + 8 \times 7.91 \times 10^{-11} + 12 \times 3.0 \times 10^{-10} + 14 \times 2.01 \times 10^{-11}) \times 6.02 \times 10^{23}}{2.1 \times 10^{16}} \times 100\,\% = 13.33\,\%$$

P: The optical power.

λ: The wavenumber of the incident light.

c: The speed of light.

h: Planck constant.

5. *In situ* diffuse reflectance infrared Fourier transform spectroscopy (DRIFTS).

In situ DRIFTS analysis was carried out in two sequential steps in a continuous-flow mode. Firstly, the catalysts were desorbed for 1 h in the N_2 atmosphere under 200 °C. Next, Data was collected in a continuous steam-saturated high purity carbon dioxide flow for 30 min at 4 cm^{-1} resolution and 128-time points were recorded under 150 °C for each experiment, with and without the LED light (420 nm) illumination. It should be noted that the background was collected in the N_2 atmosphere under 150 °C to exclude the effect of residues on the catalyst surfaces.

6. Supplementary data and figures.

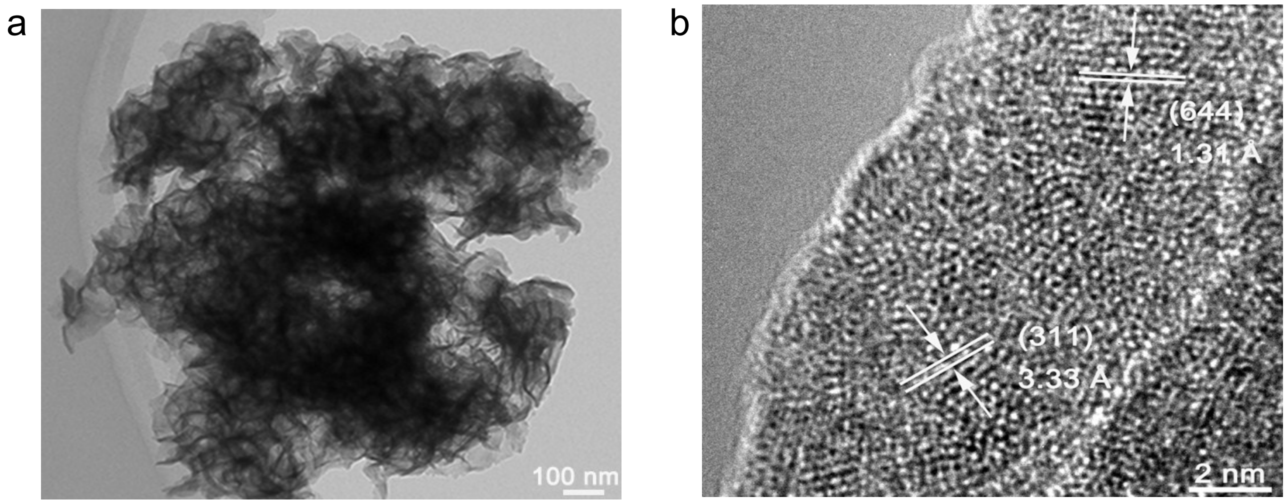

Figure S1. TEM (a) and HRTEM (b) images of C-In_2S_3.

Figure S1a reveals the morphology of C-In_2S_3. Figure S1b shows that the lattice fringes of (311) plane of C-In_2S_3 become disordered after doping with carbon.

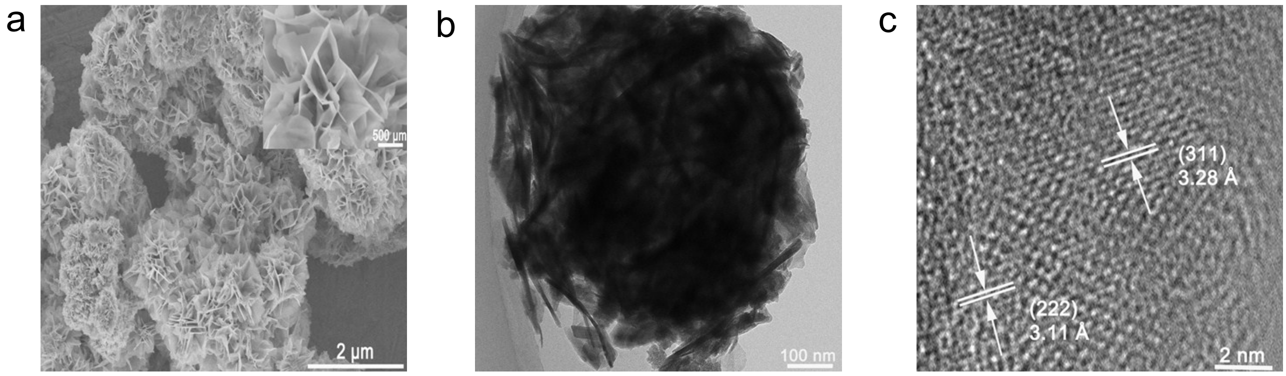

Figure S2. SEM (a), TEM (b) and HRTEM (c) images of In_2S_3.

Figure S2 reveals that the morphology of In_2S_3 is the same as C-In_2S_3 and the orderly lattice of In_2S_3 without carbon doping.

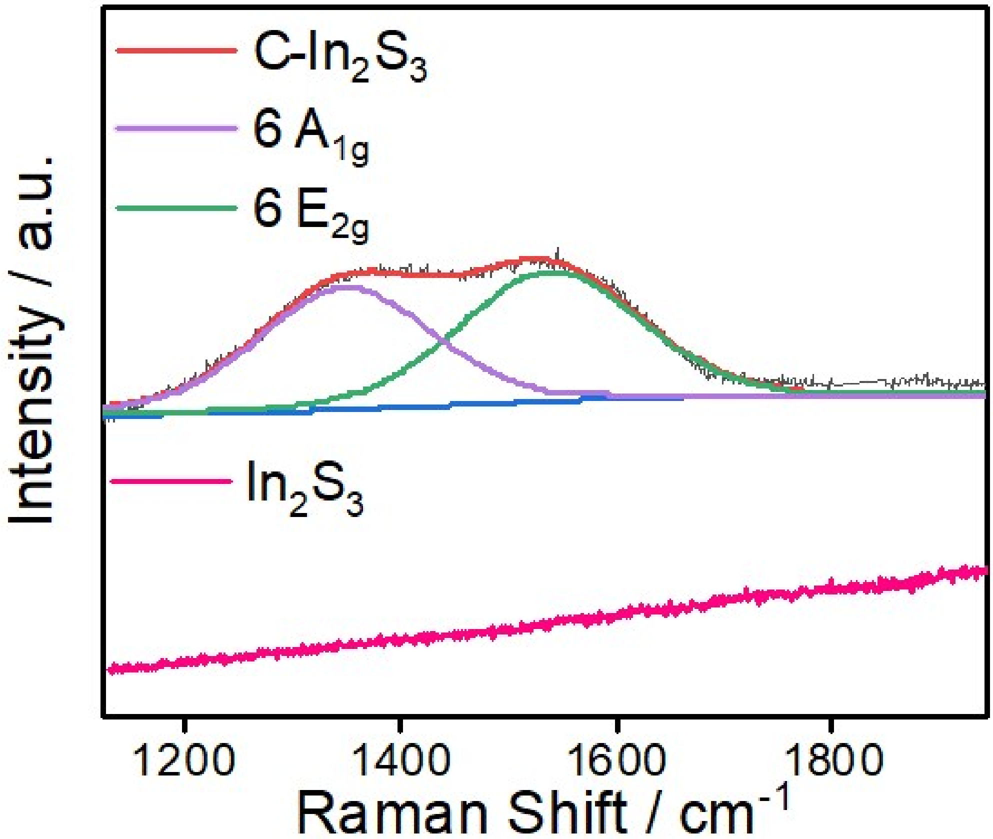

Figure S3. Carbonaceous matters analysis of the C-In_2S_3 and In_2S_3 by Raman spectra.

Figure S3 shows the Raman spectra of C-In_2S_3 reveals additional peaks ~1340, and 1525 cm^{-1}, which matches the characteristic vibrational modes of 6 A_{1g}, and 6 E_{2g}, respectively, in doped amorphous carbon with pentatomic and heptatomic rings.[3] And the In_2S_3 sample did not show any characteristic peak at 1200-1600 cm^{-1} (Figure S3), which indicates that the non-carbon-doped In_2S_3 did not form any carbonaceous materials.

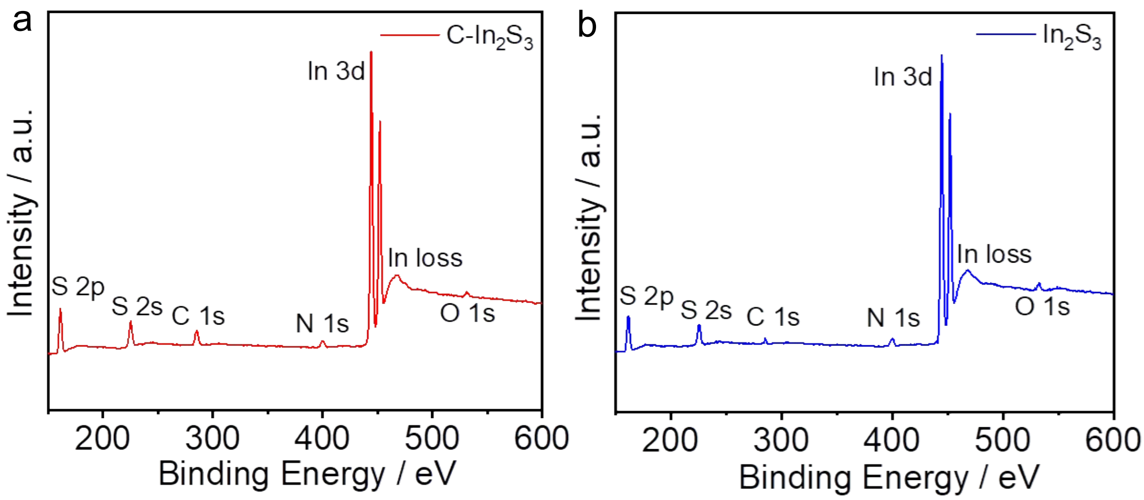

Figure S4. The XPS spectra for survey scan of C-In_2S_3 (a) and In_2S_3 (b).

To prove the impact of C doping instead of N doping, we performed the XPS spectra for a survey scan of C-In_2S_3 and In_2S_3. The N element can be detected from the XPS spectra of both samples in Figure S4. It can be seen from the XPS spectra that the intensity of the N 1s peak is almost the same in both samples, but C-In_2S_3 has a stronger C 1s peak than In_2S_3. The signals for N may come from the XPS chamber during the measurements. So, we ignore the effect of N doping, and the dominant effect of C doping leads to the differences of product distributions between our two samples. Additionally, the N doping effect was often ignored in the other reports.[4]

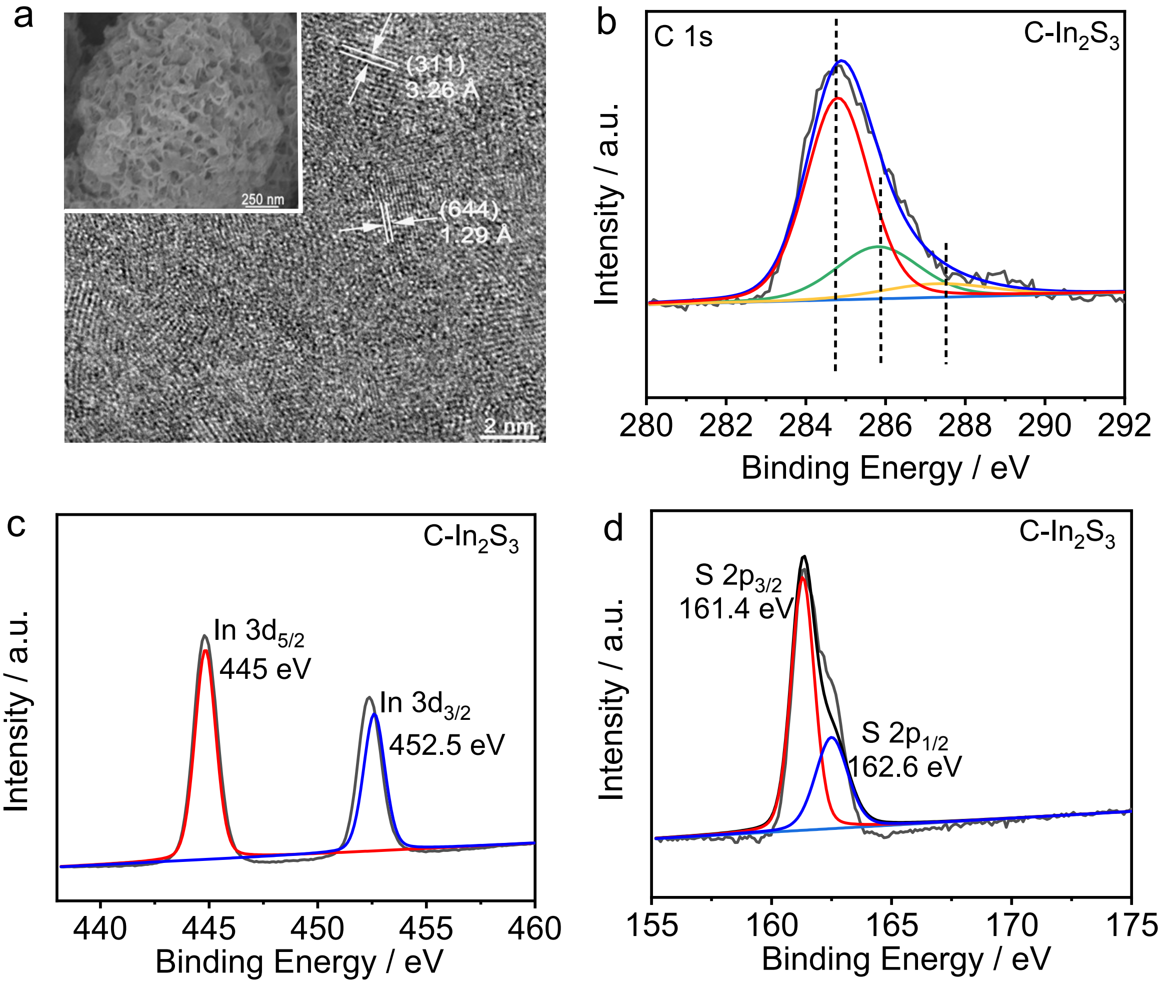

Figure S5. The (a) SEM (inset) and HRTEM after CO_2 reduction test for five cycles at 150°C, (b-d) XPS spectra for C 1s (b) In 3d (c) S 2p survey scan (d) after CO_2 reduction test for five cycles at 150°C

Figure S5 shows the SEM, HRTEM image and XPS spectra for C 1s, In 3d and S 2p survey scan of C-In_2S_3 after long-term CO_2 reduction test at 150°C. These results demonstrate that the C-In_2S_3 catalyst preserves its morphology and components after a long-term CO_2 reduction test.

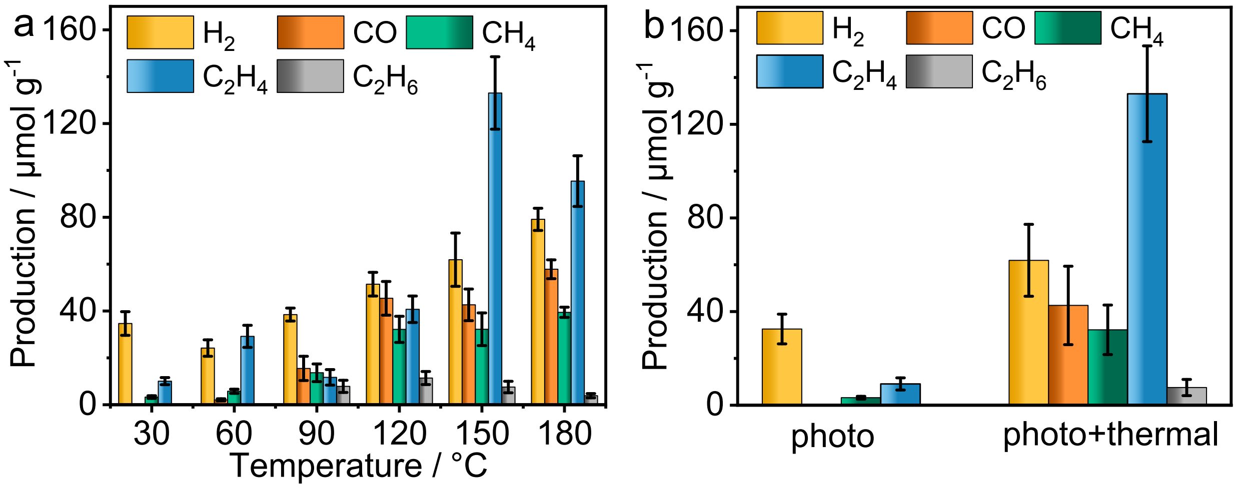

Figure S6. (a) The CO_2-H_2O reduction performances of C-In_2S_3 at different temperatures for five hours. (b) The product distribution of C-In_2S_3 reacted for five hours of photocatalytic and thermal assisted photocatalytic, respectively.

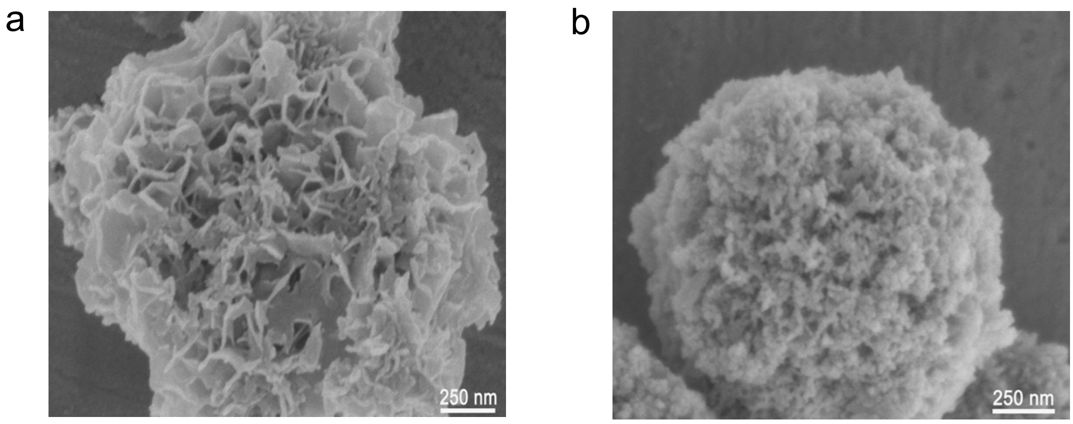

Figure S7. SEM image after CO_2 reduction test for (a) one cycle and (b) five cycles at 180 °C.

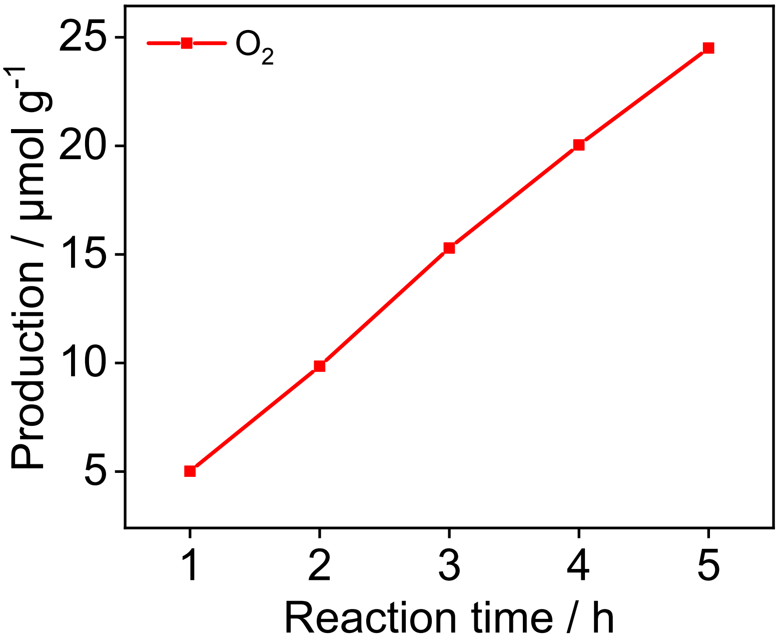

Figure S8. The production of O_2 as a function of the reaction time of C-In_2S_3 under room temperature and slightly negative pressure in an online quartz reactor.

To demonstrate the overall photocatalytic mechanism, the evolution rate of oxygen as the oxidation product under room temperature and slightly negative pressure in an online quartz reactor was measured. Figure S8 showed the O_2 evolution rate of C-In_2S_3. The O_2 evolution rates over C-In_2S_3 were 4.9 μmol g^{-1} h^{-1}, equivalent to 39.2 μmol g^{-1} h^{-1} of electrons, respectively. In the reduction reaction, the C-In_2S_3 consumed about 13.87, 5.22 and 24.16 μmol g^{-1} h^{-1} of electrons, respectively, to produce H_2, CH_4, and C_2H_4 under room temperature. The electrons from the water oxidation were almost comparable to the consumed electrons for the reduction reaction on the C-In_2S_3. This result demonstrated that H_2O as an electron donor in the whole photocatalytic process.

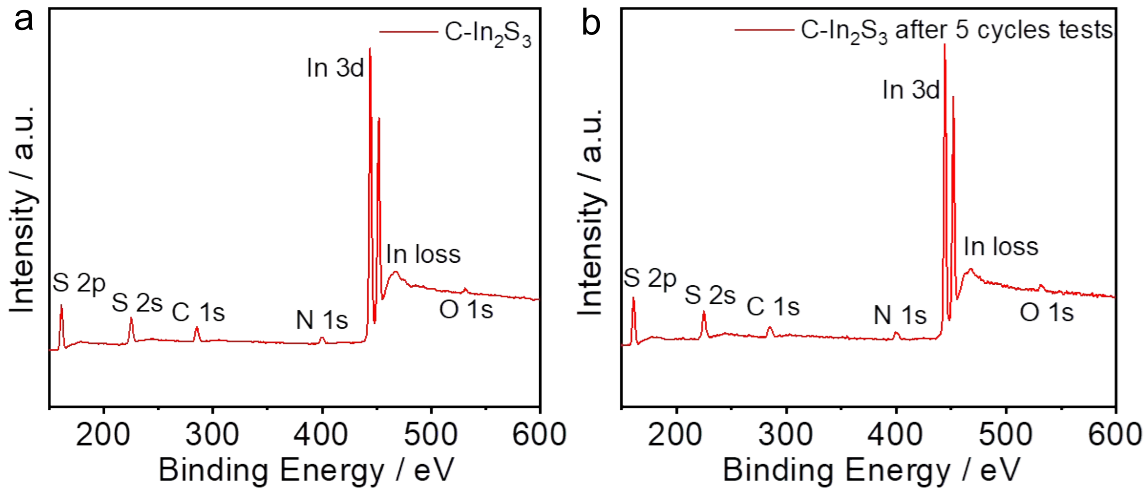

Figure S9. The XPS spectra for a survey scan of C-In_2S_3 (a) before and (b) after five cycles of photocatalytic conversion.

We did not detect any oxidation products other than O_2 in the product. This also confirms that the water acts as the electron donor and photocatalytic water splitting provides hydrogen source for C_2H_4.

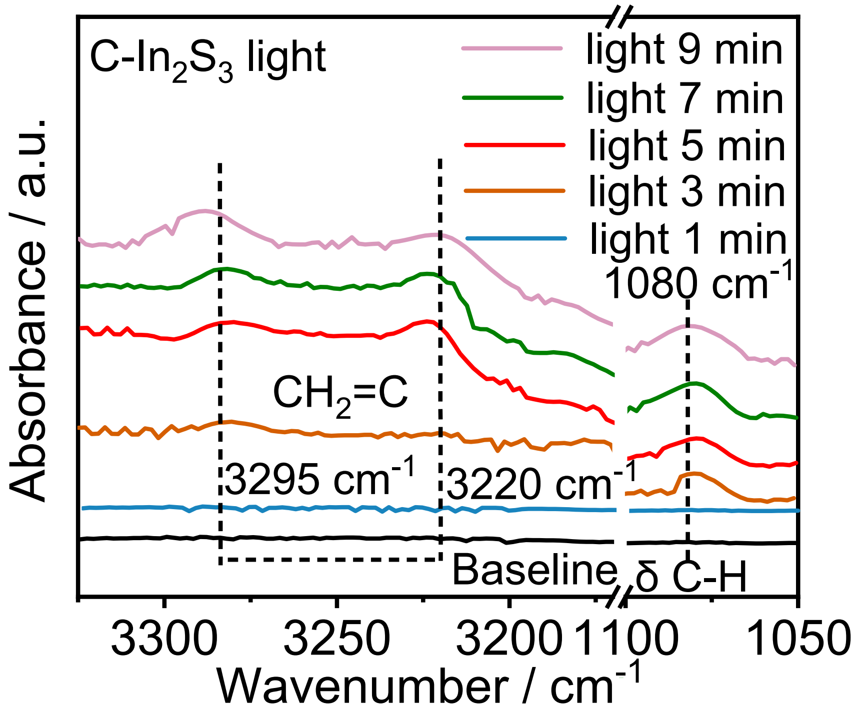

Figure S10. *In situ* DRIFTS spectra for CO_2 / H_2O vapor adsorption on C-In_2S_3 under Visible light irradiation at different times.

Computational calculations

The Materials Studio software was supported by the National Supercomputing Center in Shenzhen. Performing spin-polarization first-principles calculation based on Density Functional Theory (DFT) using CASTEP.[5] The description of exchange-correlation energy was utilized the Perdew-Burke-Ernzerhof (PBE) exchange-correlation-function[6] of the generalized gradient approximation (GGA). For the pseudopotentials, the projector-augmented-wave (PAW)[7] method was adopted. Setting 450 eV as the energy cutoff for the plane-wave basis expansion. Setting the force on each atom to 0.05 eV / Å for the convergence criterion. In order to avoid layer-to-layer interaction, the slab model was constructed with a 15 Å vacuum layer in the z-direction. According to the Monkhorst-Pack method,[8] the sampling in the Brillouin zone was set with 1×2×1. The van der Waals interaction was considered using the DFT-D3 scheme.[8] In_2S_3 was simulated by a slab p(1×1)-(311) surface with a thickness of ~ 9 Å, with five bottom layers fixed to represent the bulk features during geometry optimization and reaction calculations. The surface is dominated by three-coordinated In and S, which termination can minimize the dangling bonds. Carbon dopants are introduced to replace sulphur at the sublayers, without directly bonding with CO_2 and other intermediates, but dopants can affect the local geometries and electronic structures of surface atoms. The Computational models are displayed following:

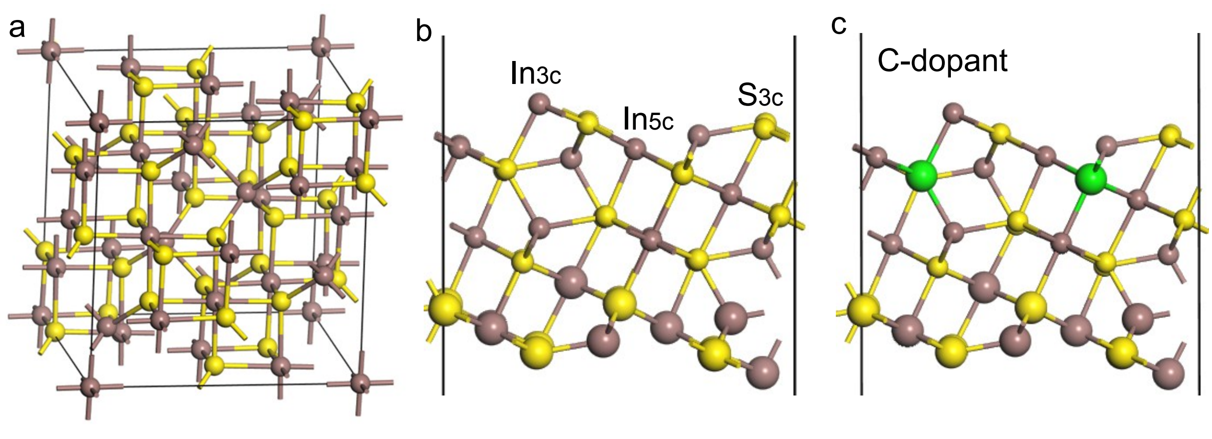

Figure S11. The Computational models of In_2S_3 (a, b) and C-In_2S_3 (c).

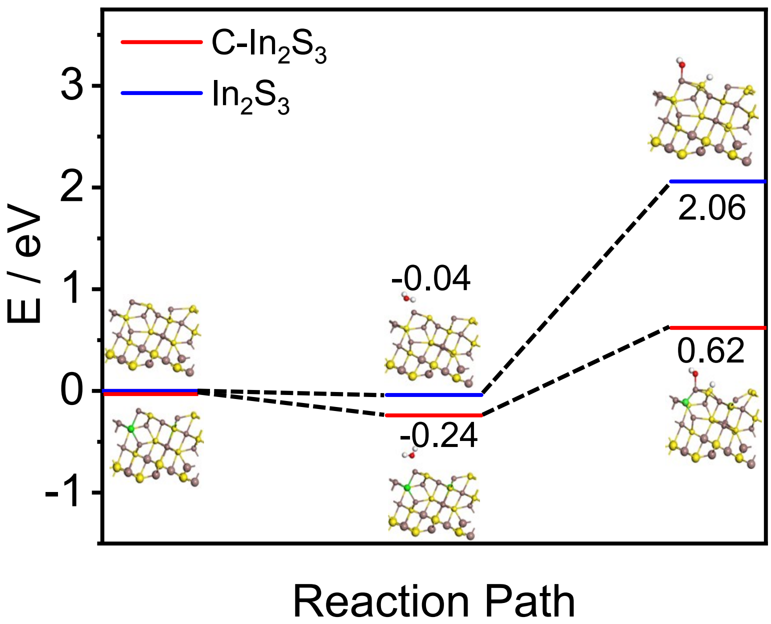

Figure S12. Calculated reaction energy diagram of H_2O to H* + OH* over C-In_2S_3 and In_2S_3.

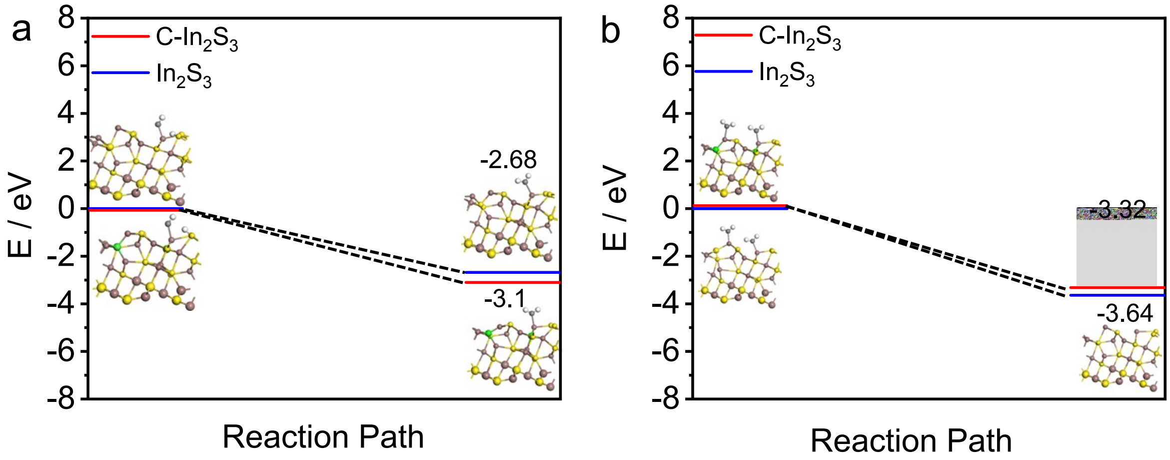

Figure S13. Calculated reaction energy diagram of CH* to CH_2* (a) and $2CH_2$* to C_2H_4 (b) over C-In_2S_3 and In_2S_3.

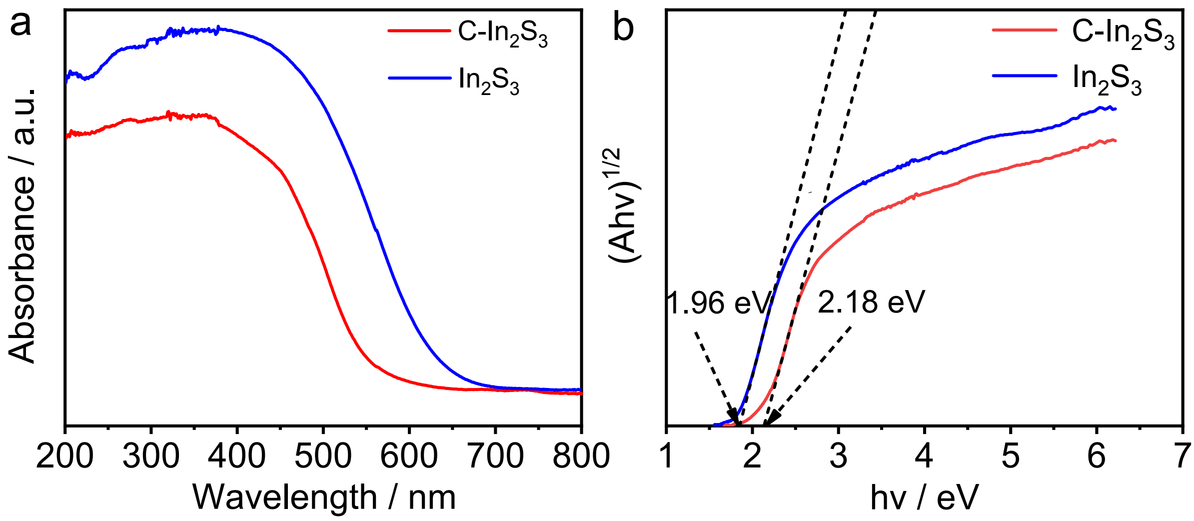

Figure S14. Uv-Vis diffuse reflectance (a) and Tauc plots with both direct and indirect fittings (b) of C-In_2S_3 and In_2S_3.

Figure S14 shows that the (*E*g) of In_2S_3 and C-In_2S_3 are obtained to be 1.96 and 2.18 eV by fitting the Uv-Vis diffuse reflectance spectrum with a modified Kubelka-Munk function.

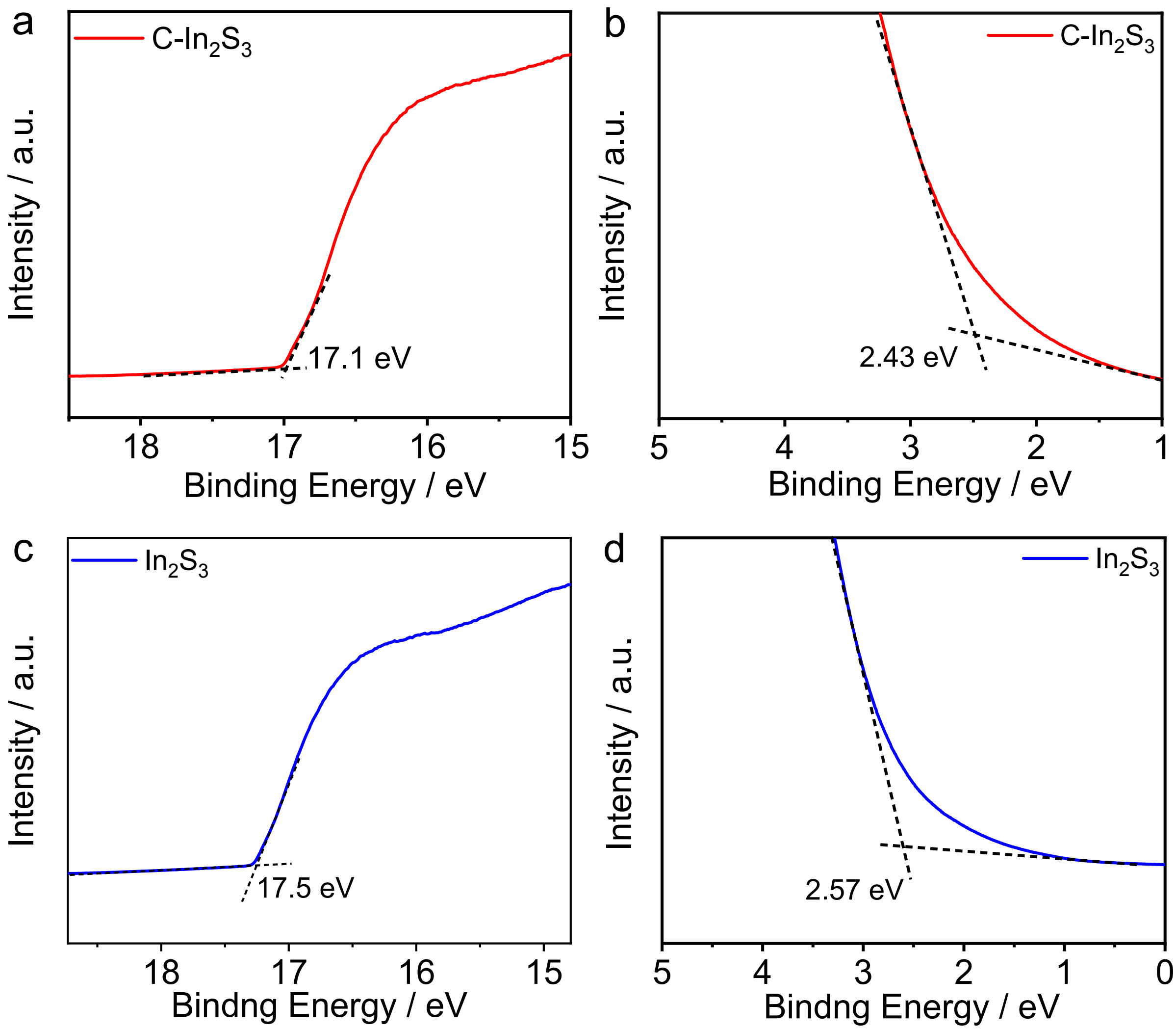

Figure S15. Ultraviolet photoemission spectroscopy (UPS) study in the cutoff (a) and the onset energy (b) regions of C-In_2S_3 and In_2S_3 (c, d). (UV light source is He I, 21.2 eV (80 mA, 530 V, 5.0 x 10^{-2} mbar): valence band, with 0 eV binding energy corresponding to the Fermi level.)

We carried out the study of ultraviolet photoemission spectroscopy (UPS) (Figure S15). The valence band of C-In_2S_3 is 1.28 eV, which is more positive than the valence band of 1.24 eV of In_2S_3, which indicate that C-In_2S_3 has a stronger ability to oxidize H_2O.[9]

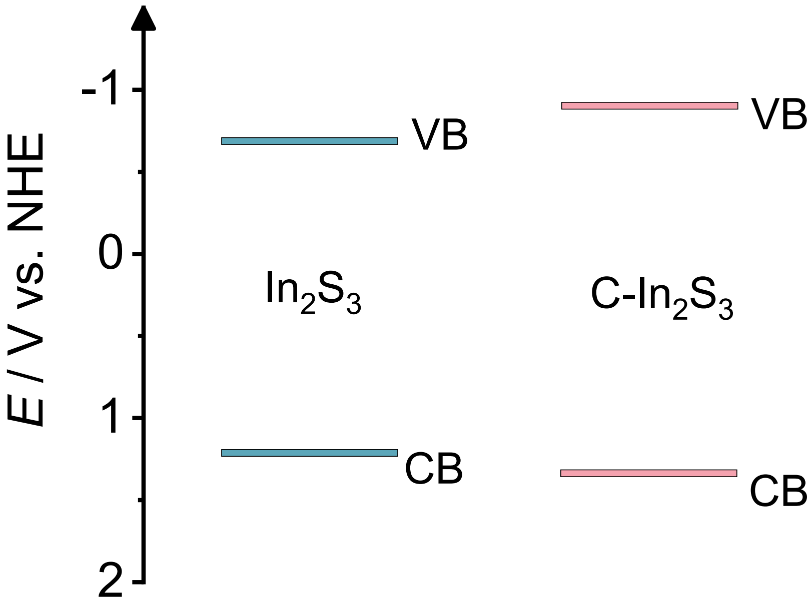

Figure S16. Schematic illustration of the band structure of In_2S_3 and C-In_2S_3.

Changing the band structure of a material has an important effect on adjusting the redox properties of the material. The band structure of In_2S_3 and C-In_2S_3 was confirmed by the results of the Uv-Vis diffuse reflectance spectra (Figure S14) and ultraviolet photoemission spectra (Figure S15), as shown in Figure S16. We adjust the bandgap of the semiconductor by introducing carbon in indium sulfide. After doping with carbon, it was found that the bandgap of In_2S_3 became wider and the conduction band position became more negative, so it had a stronger ability to reduce CO_2, while the valence band position was higher with the ability to oxidize water enhanced. Both the reductive and oxidative ability of catalysts can be enhanced after carbon doping, benefiting the multi-electron reduction process.

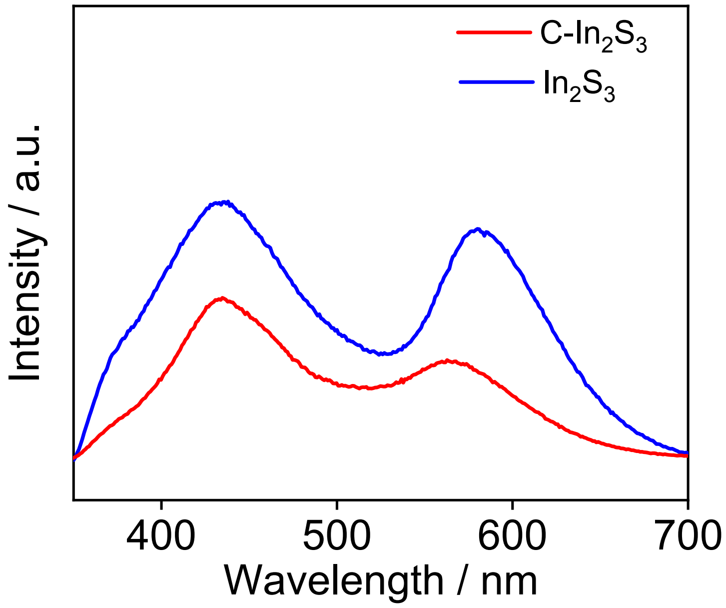

Figure S17. Spectroscopy Photoluminescence (PL) of C-In_2S_3 and In_2S_3.

To evaluate the composite ability of photogenerated charge carriers of prepared C-In_2S_3 and In_2S_3, the determination of photoluminescence (PL) was performed. The corresponding peaks at around 450 nm and 580 nm of C-In_2S_3 are relatively weaker than that of In_2S_3 (Figure S17), indicating that the photoinduced carrier recombination is greatly reduced, which may be due to carbonaceous matter and the interface charge transfer between C-In_2S_3 is enhanced.

Table S1. The total consumed electron number (TCEN) for CO_2 conversion of the C-In_2S_3 and other semiconductors.

Photocatalyst	Condition	Light source	H_2 (μmol g^{-1} h^{-1})	CO (μmol g^{-1} h^{-1})	CH_4 (μmol g^{-1} h^{-1})	C_2H_4 (μmol g^{-1} h^{-1})	C_2H_6 (μmol g^{-1} h^{-1})	CH_3OH (μmol g^{-1} h^{-1})	TCEN (μmol g^{-1} h^{-1})
C-In_2S_3	CO_2 +H_2O	UV-Vis	14.6	10.0	7.9	30.0	2.1		472.7
CdS/Ni_9S_8/Al_2O_3[10]	CO_2 +H_2O	Visible light	841.0	121.0					242.0
$ZnIn_2S_4$[11]	CO_2 +H_2O	Simulated sunlight		33.2					66.4
TiO_2-graphene[12]	CO_2 +H_2O	Full light		5.2	26.7				224.0
TiO_2/g-C_3N_4[13]	CO_2 +H_2O	Visible light		0.8	5.2				43.2
Ag/TiO_2[14]	CO_2 +H_2O	Visible light			1.7				13.6
Pt/GaN[15]	80 kPa CO_2 +H_2O	Full light		~50.0	~14.8				218.4
WN-WO_3[16]	CO_2 +H_2O	Simulated sunlight	368.5	15.2	40.6				355.2
CdS–WO_3[17]	CO_2 +H_2O	Visible light			1.0				8.2

Table S2. Chemical compositions of C-In_2S_3 and In_2S_3

Sample \ Element	In	S	C
C-In_2S_3	34.93	53.88	11.18
In_2S_3	38.74	58.12	3.14
Error±2-3 %（atomic %）			

Table S3. The chemical composition of C-In_2S_3 after five consecutive cycles.

Element / Sample	In	S	C
C-In_2S_3	36.03	54.02	9.93
Error±2-3 % (atomic %)			

Table S4. The catalytic activity of CO_2 conversion on C-In_2S_3 under different conditions

Feed gas	illumination	Temperature (℃)	Production (μmol g^{-1} h^{-1})				
			H_2	CO	CH_4	C_2H_4	C_2H_6
CO_2+H_2O	sun light	Room temperature	34.68	trace	3.26	10.07	trace
CO_2+H_2O	sun light	150	61.89	42.62	32.22	133.05	7.54
CO_2+H_2O	dark	150	trace	1.74	n.d. [a]	n.d. [a]	n.d. [a]
CO_2+H_2	dark	150	/ [b]	0.97	n.d.[a]	n.d.[a]	n.d.[a]

[a]: n.d.= not detectable. [b]: hydrogen is not quantified due to the presence in the feed gas.

References

(1) R. Wu, Y. Xu, R. Xu, Y. Huang, B. Zhang, *J. Mater. Chem. A* 2015, **3,** 1930-1934.

(2) S. Y. Li, Z. N. Du, Y. C. Zhang, *Adv. Mater. Res.* 2010, **152,** 63-66.

(3) T. E. Doyle, J. R. Dennison, *Phys. Rev. B* 1995, **51,** 196-200.

(4) 39 I. Shown, S. Samireddi, Y. C. Chang, R. Putikam, P. H. Chang, A. Sabbah, F. Y. Fu, W. F. Chen, C. I. Wu, T. Y. Yu, P. W. Chung, M. C. Lin, L. C. Chen, K. H. Chen, *Nat. Commun.* 2018, **9**, 169.

(5) S. J. Clark, M. D. Segall, C. J. Pickard, P. J. Hasnip, M. J. Probert, K. Refson, M. C. Payne, *Z. Kristallogr.* 2005, **220,** 567-570;

(6) J. P. Perdew, J. A. Chevary, S. H. Vosko, K. A. Jackson, M. R. Pederson, D. J. Singh, C. Fiolhais, *Phys. Rev. B* 1992, **46,** 6671-6687.

(7) P. E. Blochl, *Phys. Rev. B* 1994, **50,** 17953-17979.

(8) (a) H. J. Monkhorst, J. D. Pack, *Phys. Rev. B* 1976, **13,** 5188-5192;(b) S. Grimme, J. Antony, S. Ehrlich, H. Krieg, *J. Chem. Phys.* 2010, **132,** 154104.

(9) C. H. Ihara, H. Abe, S. Endo, T. Irie, *Solid State Commun.* 1978, **28,** 563-565.

(10) S. Li, Q. Wang, X. Yan, H.-Q. Zhuang, C. Yuan, J. Feng, M. Wang, R. Li, W. Li and Y.-X. Pan, *Appl. Catal. B: Environ.* 2019, **240,** 174-181.

(11) X. Jiao, Z. Chen, X. Li, Y. Sun, S. Gao, W. Yan, C. Wang, Q. Zhang, Y. Lin, Y. Luo and Y. Xie, *J. Am.Chem. Soc.* 2017, **139,** 7586-7594.

(12) M. Xu, X. Hu, S. Wang, J. Yu, D. Zhu and J. Wang, *J. Catal.* 2019, **377,** 652-661.

(13) K. Li, B. Peng, J. Jin, L. Zan and T. Peng, *Appl. Catal. B: Environ.* 2017, **203,** 910-916.

(14) S. Feng, M. Wang, Y. Zhou, P. Li, W. Tu and Z. Zou, *APL Mater.* 2015, **3,** 104416.

(15) B. AlOtaibi, S. Fan, D. Wang, J. Ye and Z. Mi, *ACS Catal.* 2015, **5,** 5342-5348.

(16) D. L. Liu, C. H. Wang, Y. F. Yu, B. H. Zhao, W. C. Wang, Y. H. Du, B. Zhang, *Chem* 2019, **5,** 376-389.

(17) J. Jin, J. Yu, D. Guo, C. Cui and W. Ho, *Small* 2015, **11,** 5262-5271.